Diluted Chemical Identification by Total Internal Reflection Photonic Sensing
Biomedical Optics

Eduardo Valero, Sergio L. Carrasco-Ortiz, Maria Morant and Roberto Llorente
Nanophotonics Technology Center, Universitat Politècnica de València, Camino de Vera s/n, Valencia, Spain

Keywords: Photonic Sensor, Bio-chemical Sensing, Image Processing.

Abstract: A novel optical sensor architecture for the rapid identification of liquid samples is proposed and evaluated experimentally. The proposed architecture is based on total internal reflection transmission of a laser beam. A CMOS sensor is used to acquire the reflection produced by a narrow laser beam when interacting with the liquid sample on the surface of an equilateral prism. Using digital image processing techniques, the critical angle of the transmission is calculated and the identification of the refractive index of the liquid sample is obtained. In the present work, distinct liquid substances were evaluated experimentally using a red He-Ne laser at 632.8 nm wavelength obtaining the refractive index with a deviation of less than 0.0014 from the value. Sensing by refractive index changes are of great importance in biomedical (e.g. optical diagnosis and laser treatments) and chemical applications.

1 INTRODUCTION

In the last decades, the design of sensors has evolved combining the fundamental biological, chemical, and physical sciences with engineering and computer science to fulfil concrete needs in a wide range of application areas (Adl et al., 2017). In both medical and industrial applications, optical biosensors have gained attention in the last years due to their simplicity and high sensitivity (Adl et al., 2017). Optical biosensors can be applied to detect early diseases (Haes et al., 2005) measure biomolecular assays (Meglinski, 2015) or industrial applications like process monitoring in plant factories (Chiu et al., 2016).

In this work, we propose and demonstrate experimentally a prism-based optical sensor for the detection and identification of the refractive index of liquid samples. The refractive index of a material is a characteristic optical parameter that describes the speed of light ratio of the material in respect of its propagation speed in vacuum. Albeit there are some techniques that have been proposed for measuring the refractive index (Lai et al., 2005), the majority are based on the measurement of light intensity fluctuations by a photodetector (Li and Xie, 1996). Furthermore, there have been proposed several techniques based on the total internal reflection (TIR) (Sainov, 1994) which demands the use of a precise goniometer and its calibration (Onofri et al., 2007). The proposed sensor is based on TIR propagation, which permits detection of changes in the beam position or refractive index variations caused by the biological sample interacting in the sensor surface (Watad et al., 2015). The sensor is intended to be integrated close to the optics in conventional CCD camera, as found in today's cellphones, targeting a cost-effective implementation of a complete bio-chemical identification system.

The proposed prism-based sensor concept is described in Figure 1, where a laser beam propagates through a medium with high refraction index (i.e. the prism with refractive index n_{prism}) and encounters a planar interface with a medium of lower refraction index (water or other liquid sample with $n_{sample} < n_{prism}$). Total internal reflection occurs for incidence angles greater than the critical angle ($\theta_i > \theta_c$) (Uddin and Talukder, 2016).

Following this approach, in this work we measure experimentally different liquid samples, searching TIR transmission in a prism to obtain the critical angle for each substance. In these experiments, the critical angle is measured by means of the acquisition of frames with a high-speed camera located

Valero, E., Carrasco-Ortiz, S., Morant, M. and Llorente, R.
Diluted Chemical Identification by Total Internal Reflection Photonic Sensing - Biomedical Optics.
DOI: 10.5220/0006616501970204
In *Proceedings of the 6th International Conference on Photonics, Optics and Laser Technology (PHOTOPTICS 2018)*, pages 197-204
ISBN: 978-989-758-286-8

orthogonally to the plane of propagation using proper digital image processing techniques as described in this paper which avoids the need of calibrating the system with a precise goniometer. The accurate determination of critical angle on different substances may result on more reliable tissue characterization for diagnostics purposes (Knüttel and Boehlau-Godau, 2000).

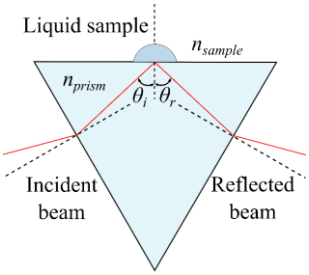

Figure 1: Proposed microprism-based sensor (refractive index n_{prism}) for the critical angle calculation of a laser beam transmission interacting with liquid samples (refractive index n_{sample}).

This paper is structured as follows: In Section 2, the theoretical principles of critical angle in TIR transmission are summarized. Next, in Section 3, simulations solving the Fresnel equations and the Stokes parameters were carried out in order to compare with the experimental results performed in the laboratory depicted in Section 4. In Section 4, the digital processing algorithms developed for the calculation of the critical angle (θ_c) and the experimental results obtained for identifying the refractive index of the sample (n_{sample}) are reported. Finally, Section 5 highlights the main conclusions.

2 PRISM-BASED OPTICAL SENSOR FOR REFRACTIVE INDEX IDENTIFICATION

2.1 Total Internal Reflection

Refraction is a physical phenomenon by which an electromagnetic wave changes its direction a certain angle θ as a consequence of a change in the velocity of its medium of propagation (Hecht, 2002). Figure 2 describes the principles of reflection and refraction at the interface of two materials with different refractive indexes (n_{prism} and n_{sample}) defined by the Snell's Law. Considering that θ_i and θ_r the incident and reflected angles respectively, then, according to the Snell's law of reflection the angles of reflection and incidence are equal (Wang et al., 2016).

$$\theta_i = \theta_r \tag{1}$$

Moreover, the Snell's law of refraction defines the relationship between the angle of incidence θ_i and the transmitted angle θ_t:

$$n_{prism}\, sin\, \theta_i = n_{sample}\, sin\, \theta_t \tag{2}$$

If the light is coming from a denser to a lighter material, the transmission angle can take its maximum value –also known as the critical angle of incidence θ_c– and, instead of passing through to the second medium, the transmitted beam is reflected at the interface to stay in the first medium. This critical angle θ_c can be calculated as:

$$\theta_c = sin^{-1}\frac{n_{sample}}{n_{prism}} \tag{3}$$

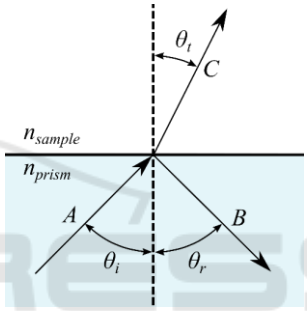

Figure 2: Snell's law for light reflection and refraction at the interface of two materials.

2.2 Principle of Operation

In the proposed architecture, an equilateral prism is used to find the critical angle and calculate the refractive indexes of the substances on its sample interface on top. The beam angle of incidence (θ_i) is adjusted in order to reach the critical angle (θ_c) achieving TIR transmission inside the prism.

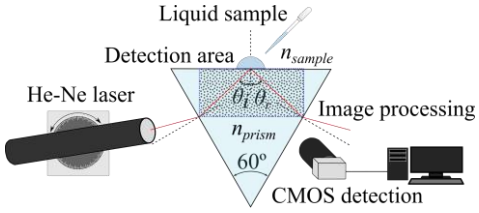

Figure 3: Experimental setup for the calculation of the refractive index of liquid samples (n_{sample}) by means of TIR and CMOS detection of the incident (θ_i) and reflected angles (θ_r) with image processing.

Figure 3 shows the experimental setup for the evaluation of the proposed architecture employing an

equilateral prism (60º between faces). A goniometer with a He-Ne laser with linear polarization in the visible red spectrum (λ = 632.8 nm) is employed to modify the incident angle θ_i. This incident laser beam interferes with the sample solution (n_{sample}) at the prism top surface. When the incident angle is adequate, the beam is TIR reflected back to the prism with a reflected angle θ_r. These angles (θ_i and θ_r) are detected by a complementary metal-oxide-semiconductor (CMOS) sensor array comprising 1280×1024 pixel cells. Applying equations (2) and (3) to the prism-based sensor depicted in Figure 3, knowing the refractive index of the prism (n_{prism}) and the propagation angles (θ_i and θ_r) we obtain the refractive index of the sample (n_{sample}) as:

$$n_{sample} = n_{prism} \frac{sin\,\theta_i}{sin\,\theta_r} \quad (4)$$

Moreover, then TIR is achieved, there is also a change in the polarization of the wave. This change is produced because the component waves experience different phase shifts δ_p and δ_s for the waves of incident light linearly polarized parallel (p) and perpendicular (s) (Azzam, 2004). Therefore, a linearly polarized wave becomes elliptically polarized when is reflected with an angle of incidence greater than the critical angle (Haus, 2016).

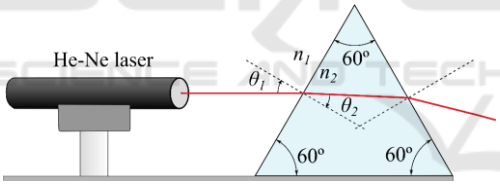

Figure 4: Schematic diagram for the calculation of the refractive index of the prism.

Since the refractive index of the prism was not provided by the manufacturer, we measured it experimentally using the setup described in Figure 4. The He-Ne laser (JDSU 1135P) is oriented into the equilateral prism (Eisco Labs PH0554GG) with an 90º angle to the normal vector of the optical table. Applying Snell's law and knowing the refractive index of air (Ciddor, 1996) and the incident angle, we measure the transmission angle to be θ_t=19.5174º. Thus, the value obtained for the refractive index of the prism was $n_{prism} = 1.4970$ which corresponds to Phosphate Crown PK SCHOTT glass N-PK52A (SCHOTT North America, Inc, 2015).

In this experimental demonstration, several liquid substances were employed to assess the performance of the proposed sensing method: water (H_2O), 2-propanol ($CH_3CHOHCH_3$), absolute ethanol (CH_3CH_2OH), hydrogen peroxide (H_2O_2) and olive oil. The values of the refractive index of these substances are summarized in Table 1 according to the literature for water (Hale and Querry, 1973), 2-propanol (Sani and Dell'Oro, 2016), ethanol (Sani and Dell'Oro, 2016), hydrogen peroxide (Phibbs and Giguère, 1951) and olive oil (Yunus et al., 2009).

Table 1: Refractive index of the substances under study for 25 ºC room temperature.

Substance	Refractive index (n_{sample})
Water	1.3317
2-propanol	1.3763
Ethanol	1.3598
Hydrogen peroxide	1.4067
Olive oil	1.4650

2.3 Beam Digitization

The incident and the reflected beams are detected with the CMOS sensor with a dynamic range of 62.1 dB, a dark temporal noise lower than 9 e^- and a Signal to Noise Ratio of 40 dB (On-Semi Python 1300) with an optical lens with a focal length of f = 25 mm (KOWA LM25JC1MS). The pixel size of the sensor CMOS is of 4.8 µm, hence the width of the laser beam detected (being its size of 0.68 mm and its divergence of 1.2 mrad) is digitized with a width of S_i = 21 pixels as depicted in Figure 5.

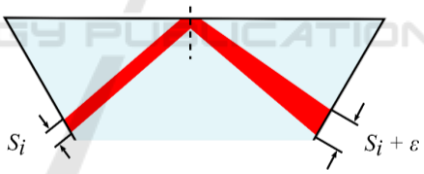

Figure 5: Schematic diagram of the divergence of the laser beam travelling inside the prism.

The angle of incidence of the beam is estimated using image processing techniques with MATLAB. In order to obtain a correct estimation is important that the width of the laser digitized is maintained, and is not superior to the initial value S_i. This should be noted because the laser beam diameter increases with distance propagated from the optical source; this effect is known as divergence (Sliney and Wolbarsht, 1980). We can obtain the divergence (Φ) of a laser beam, knowing the beam diameter at two points (D_i and D_f) separated a distance (l) as:

$$\Phi = \frac{D_f - D_i}{l} \quad (5)$$

With the proposed optical sensing technique to calculate the incident and reflected angles, an could

be originated when the original size of the laser beam (S_i) increases one pixel (ε). Each pixel of the image acquired in these experiments is equivalent to a length of 0.04 mm. Applying equation (5), the distance to obtain this increment in the diameter of 0.04 mm would be of 33.33 mm, resulting in the increment of one pixel when digitized.

This increment can cause an error in the estimation of the concentration of the liquid sample. The relative error in the estimation of the angle of incidence with MATLAB for a beam with divergence, with regard to the same beam without divergence, was calculated to be as small as 0.018%.

In this case, the prism used for the experimental validation has a dimension of 25×25×22 mm, and it is designed to be able to measure the refractive indexes in the range from 1.3317 to 1.4741.

For example, for the refractive index of n_{sample} = 1.3317, the beam travels a distance of 21.70 mm which entails an increment of 0.65 pixels. While for the refractive index of n_{sample} = 1.4741, the beam travels a distance of 23.04 mm, resulting in an increment of 0.69 pixels. Thus, the increment is always less than one pixel and no error is induced by the beam digitization in the processing of the images.

3 SIMULATION RESULTS

In-depth simulation studies have been performed using COMSOL Multiphysics framework to analyse the behaviour of the angle of incidence to achieve TIR for different substances in the sensor surface. The intensity of the optical rays was computed by the Stokes parameters and the transmission and reflection coefficients at the boundary of the mediums were calculated applying the aforementioned Fresnel equations.

3.1 TIR Propagation in the Prism

Following the experimental setup depicted in Figure 3, an equilateral prism is considered in the simulation studies with a refractive index of n_{prism}=1.4970, according to the results reported in Section 2.2 of this paper. The simulation studies were carried out using an optical laser at 633 nm in the red visible spectrum. The angle of the laser beam was iteratively modified to ascertain the critical angle.

Figure 6 shows the simulation results obtained for a semi-spherical bubble of ethanol with refractive index $n_{ethanol}$=1.3598 present in air environment. For ethanol, the theoretical critical angle according to equation (3) is calculated as:

$$\theta_{c\_ethanol} = sin^{-1}\frac{n_{ethanol}}{n_{prism}} = 65.2783^{o} \quad (6)$$

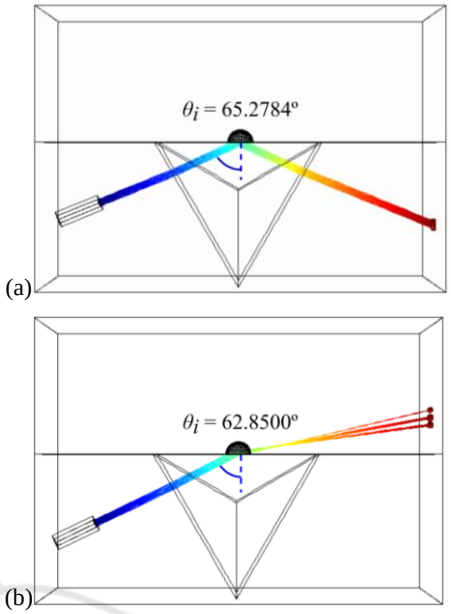

Figure 6: Incident angle simulation results obtained for an ethanol bubble when the incident laser beam angle is: (a) superior to the critical angle θ_i=65.2784º and (b) smaller than the critical angle θ_i=62.8500º.

As depicted in the simulation results represented in Figure 6(a), when the angle of incidence is higher to the critical angle ($\theta_i > \theta_{c,ethanol}$), the optical beam is reflected back to the prism by TIR propagation. Table 2 includes the simulated results obtained for the different liquid substances under study.

Table 2: Simulated results for critical angle calculation for each substance under study.

Substance	Critical angle (θ_c)
Water	62.8204º
2-propanol	66.8345º
Ethanol	65.2783º
Hydrogen peroxide	69.9978º
Olive oil	78.1320º

When the angle of incidence is close, but smaller than the critical angle ($\theta_i < \theta_{c,ethanol}$), the laser beam is not totally reflected and secondary rays are transmitted through the interface or to the second medium as represented in Figure 6(b).

3.2 Evaluation of Micro-prism Size

Moreover, simulations were carried out to estimate the theoretical minimum size of the prism. The beam

diameter of the laser is reduced from 480 µm to 45 µm with a beam reducer in order to minimize the dimensions of the prism. The size of the side of the prism depends on the spot size of the laser when the total internal reflection is produced. The spot size corresponding to the critical angle (θ_c) of a substance with a refractive index of n_{sample} = 1.4741 (maximum value of refractive indexes to cover with the proposed biosensor) was evaluated. The resulting spot size of 290.8 µm restricts the minimum size of the side of the prism in contact with the substance. Therefore, for these range of refractive indexes, the minimum dimensions of the prism are calculated to be 290.8×290.8×45 µm.

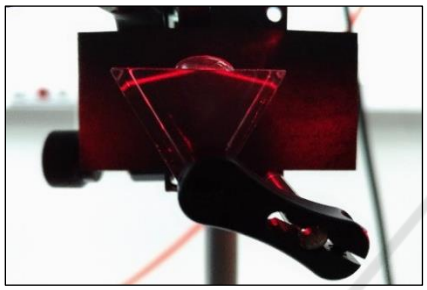

Figure 7: Laboratory caption of the experimental setup of the biosensor for the refractive index calculation of a liquid bubble by critical angle measurement.

A study of the effect of the beam divergence when digitized was carried out. For the refractive index of n_{sample} = 1.4741, that corresponds with the value more affected by divergence, the beam travels a distance of 252.41 µm, resulting in an increment of 0.11 pixels, therefore, no error is produced.

4 EXPERIMENTAL DEMONSTRATION

4.1 Laboratory Setup and Digital Image Processing

Figure 7 shows a photograph of the experimental setup developed at the laboratory for the calculation of the refractive indexes of different liquid samples using the proposed biosensor. A He-Ne laser with a wavelength of λ=632.8 nm and linear polarization (JDSU 1135P) is employed with an equilateral prism (Eisco Labs PH0554GG). To ensure that the room temperature was constant an air conditioning system was used to set it at 25 ºC and it was monitored using a thermometer to confirm that the temperature was not altered. A drop sample of the liquid substance under evaluation is located on the upper side of the prism. Images of the reflection produced by the substance were gathered with a high-speed camera with a resolution of 1280×1024 pixel and a sample rate of 80 fps employing a 25 mm lens.

Figure 8 illustrates the block diagram of the algorithm used for the calculation of the refractive index of the substances under study. In the measurement procedure, we first capture an image frame with the laser switched off to detect the exact position of the prism applying a morphological opening comprising a structuring element with the shape of a line with the same inclination as the prism. In order to optimize the detection conditions, the measurements were taken without extra illumination in the laboratory, so that the laser beam is detected with more intensity compared to the rest of the image. With this condition, the time exposure was increased to use a long-duration shutter speed of 15000 µs, hence absorbing more light from the laser beam.

In the next step, the laser is switched on and several frames are captured with the CMOS sensor while searching the critical angle by rotating the goniometer.

In order to detect the laser beams travelling through the prism, digital image processing has been programmed with MATLAB including Image Acquisition and Processing toolboxes. The main steps of the image processing consist in:

1. Foreground detection by background subtraction of the frame of the prism captured with the laser switched off.
2. Crop of the detection area in the prism where the incident and reflected beams are located.

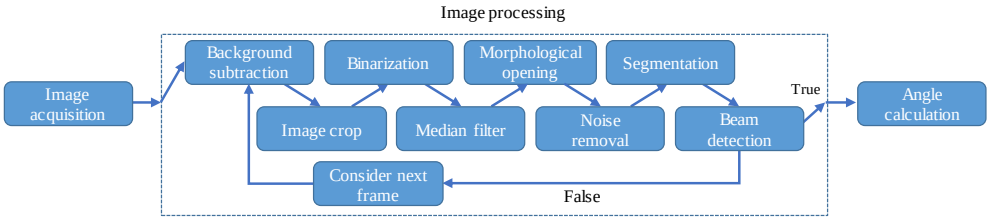

Figure 8: Process flow diagram of the developed algorithms for the calculation of the critical angle with CMOS sensing and digital image processing.

3. Binarization of the frame with an adaptive method. The pixels of the captured monochrome frame are binarized to 0 or 1 values, being the calculation of the threshold based on the first-order image statistics around each pixel. More information on adaptive image filtering can be found in (Gonzalez and Woods, 2011)
4. Coarse noise reduction by median filtering.
5. Fine noise reduction applying a morphological opening using a structuring element with the shape of a disk.
6. Filtering of objects with a small area.
7. Segmentation of the objects of the image.
8. Laser beam angle calculation on the frame after the last step in the segmentation process.

Following the aforementioned procedure, the calculation of the angle depends on the laser beams detected on the frame after the last step in the segmentation process. If the incident and reflected beams are not detected, or if there are more rays detected besides both of them, the current frame is discarded and the next frame is analysed following the same procedure.

4.2 Performance Validation

Figure 9 shows the experimental results obtained after digital image processing for a drop of water interacting with the laser beam at the surface of the prism. According to Table 1 and Table 2, the refractive index of the water is n_{water} = 1.3317 (Hale and Querry, 1973) which gives a critical angle of $\theta_{c,water}$ = 62.8204º.

As it can be observed in Figure 9(a), when total internal reflection is achieved ($\theta_i > \theta_c$), only two laser beams are detected. Thus, we are able to measure the angle of incidence (θ_i) and the angle of reflection (θ_r) and calculate the refractive index of the sample using equation (4). This method was applied four times to each of the liquid substances under study and the standard deviation of the results is calculated for all the measures reported in Table 3.

In the case of sensing water with the proposed biosensor, the experimental angle was measured to be 62.4636º ± 0.0236º, as represented in Figure 9(a).

In the second case, when the angle of incidence is below the value of the critical angle ($\theta_i < \theta_c$), we can observe in Figure 9(b) that a third beam appears in the image as a result of the energy transmitted to the second media returned to the prism. In this case, no TIR transmission is achieved and the goniometer has to be modified till obtaining the critical angle (θ_c).

Figure 10 shows the experimental results taken for 2-propanol and hydrogen peroxide with measured incident angle of $\theta_{i,2-propanol}$ = 64.4335º and $\theta_{i,hydrogen\ peroxide}$ = 69.3342º respectively.

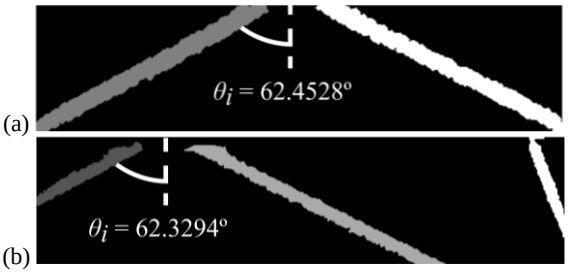

Figure 9: Examples of the detected laser beam after applying image processing when interacting with a drop of water when: (a) TIR is achieved ($\theta_{i,water}$ = 62.4528º) and (b) TIR is not achieved in this case (θ_i = 62.3294º).

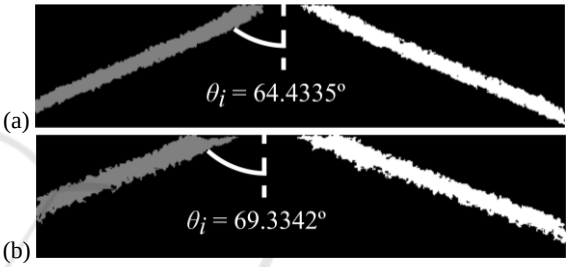

Figure 10: Experimental results and measured incident angle for: (a) 2-propanol (θ_i = 64.4335º) and (b) hydrogen peroxide (θ_i = 69.3342º).

The experimental results of mean and standard deviation for the four iterations of this sensing method are included in Table 3.

Comparing the results obtained for the refractive indexes of each substance with the values reported before in Table 1, we observe that the most accurate measurement was obtained sensing olive oil with an error of only 0.16%.

Evaluating the experimental results in Table 3, the biggest error is obtained for Hydrogen peroxide with a 0.44%. A possible reason of this calculation error can reside in the width of the beam spot of the laser. Future work on this topic will evaluate more collimated laser beams in order to reduce this error. Another reason could reside in the shape of the prism. Usually, fabrication of prisms have an angular tolerance and are not perfectly equilateral. This factor could lead to an error in the calculation of the refractive index of the prism measured previously in Section 2.2 of this paper. For this reason, we further studied this aspect to reduce the error in the detection. This and other manufacturing defects can be compensated by a calibration process.

Table 3: Experimental measurements of the angle of incidence and calculations of the refractive index of the liquid substances under study (25 ºC) considering a prism with n_{prism}=1.4970.

Substance	Measured angle (º)	Refractive index	Error
Water	62.4636 ± 0.0236	1.3274 ± 0.0003	0.0032
2-propanol	66.4762 ± 0.1184	1.3726 ± 0.0014	0.0027
Ethanol	64.9659 ± 0.0871	1.3564 ± 0.0011	0.0025
Hydrogen peroxide	69.3100 ± 0.1151	1.4005 ± 0.0012	0.0044
Olive oil	77.7154 ± 0.1418	1.4627 ± 0.0009	0.0016

4.3 Sensor Performance with Calibration

The calibration process targets to correct face angle deviations and prism refraction index manufacturing deviations. Considering a perfect calibration, we have calculated the refractive index that minimize the error to be n'_{prism} = 1.5015. The new calculations of the refractive indexes of the liquid samples considering n'_{prism} and the measured incident angles are reported in Table 4 as a best-case performance scenario for the sensor. Observing the results of Table 4 we can see that the refractive indexes of water, 2-propanol and ethanol substances are detected with only 0.02%, 0.03% and 0.05% error respectively. Considering n'_{prism} the maximum error is reduced to 0.14% and is given for hydrogen peroxide and olive oil samples.

Table 4: Refractive index calculation of the liquid substances under study (25 ºC) to reduce the error considering a prism with n'_{prism}=1.5015.

Substance	Measured angle (º)	Refractive index	Error
Water	62.4636 ± 0.0236	1.3314 ± 0.0003	0.0002
2-propanol	66.4762 ± 0.1184	1.3767 ± 0.0014	0.0003
Ethanol	64.9659 ± 0.0871	1.3604 ± 0.0011	0.0005
Hydrogen peroxide	69.3100 ± 0.1151	1.4047 ± 0.0012	0.0014
Olive oil	77.7154 ± 0.1418	1.4671 ± 0.0009	0.0014

This confirms that the accuracy of the calculation of the refractive of the prism media is essential for the correct detection of liquid samples using the proposed sensing technique.

5 CONCLUSIONS

This work presents and evaluates experimentally a prism-based biosensor capable of identifying the refractive indexes of liquid samples. This sensor is based on TIR transmission of an optical beam interacting with liquid drops on the surface of an equilateral prism. This sensing method is based on total internal reflection of the laser beam due to the change of the refractive indexes of the two media (prism and liquid sample). TIR transmission is achieved for incident angles higher than the critical angle ($\theta_i > \theta_c$).

A laser source in the visible spectrum range (in this case a red He-Ne laser operating at 632.8 nm) is transmitted through a transparent equilateral prism in order to be able to see the incident and reflected beams after interacting with the liquid sample located on the upper side of the prism. The incident angle is modified until achieving TIR transmission. The see-through face of prism is captured with the CMOS sensor of a camera and digital image processing is performed with MATLAB to obtain the incident angle values. In this work, the image processing process is described to measure the incident and reflected angles (θ_i and θ_r). From these angle values, the refractive index of the liquid sample is calculated.

The proposed sensing method based on a single prism and a CMOS sensor of a commercial camera are accurate and simple, since there is no need of a calibration with a precise goniometer as in conventional systems. This sensor is capable of identify refractive indexes in the range from 1.3317 to 1.4741. Depending on the resolution of the camera employed, the size of the prism could be reduced to micro-prism scale. The experimental results point out that the sensing accuracy of this method rely on the collimation of the laser source (beam width) and also on the material of the prims used for TIR propagation.

With proper values of the material of the prism, we were able to detect different liquid substances with an error lower than 0.14%, being capable of detecting water bubbles present in air with an error of only 0.02% and 2-propanol and ethanol samples with an error of 0.03% and 0.05%, respectively. Knowledge of the refractive index is essential for biomedical applications for optical diagnosis.

ACKNOWLEDGEMENTS

This research work was supported in part by Spain National Plan MINECO/FEDER UE RTC-2014-

2232-3 HIDRASENSE and TEC2015-70858-C2-1-R XCORE projects. BIOFRACTIVE project with IIS La Fe is also acknowledged. M. Morant work was partly supported by UPV postdoc PAID-10-16 program.

REFERENCES

Adl, H. P. et al., 2017. A Defective 1-D Photonic Crystal-Based Chemical Sensor in Total Internal Reflection Geometry. *IEEE Sensors Journal*, 17(13), pp. 4046-4051.

Azzam, R. M. A., 2004. Phase shifts that accompany total internal reflection at a dielectric–dielectric interface. *Journal of the Optical Society of America A*, 21(8), pp. 1559-1563.

Chiu, J.-S. et al., 2016. Application of Total Internal Reflection and Heterodyne Interferometry in Electrical Conductivity Measurements. *IEEE Sensors Journal*, 16(2), pp. 336-342.

Ciddor, P. E., 1996. Refractive index of air: new equations for the visible and near infrared. *Applied Optics*, 35(9), pp. 1566-1573.

Gonzalez, R. C. and Woods, R. E., 2011. *Digital Image Processing.* 3rd ed. s.l.:Pearson Education.

Haes, A. J. et al., 2005. Detection of a Biomarker for Alzheimer's Disease from Synthetic and Clinical Samples Using a Nanoscale Optical Biosensor. *Journal of the American Chemical Society*, 127(7), pp. 2264-2271.

Hale, G. M. and Querry, M. R., 1973. Optical Constants of Water in the 200-nm to 200-μm Wavelength Region. *Applied Optics*, 12(3), pp. 55-563.

Haus, J. W., 2016. *Fundamentals and Applications of Nanophotonics.* s.l.:Woodhead Publishing.

Hecht, E., 2002. *Optics, 4th. International edition.* 3 ed. San Francisco: Addison-Wesley.

Knüttel, A. and Boehlau-Godau, M., 2000. Spatially confined and temporally resolved refractive index and scattering evaluation in human skin performed with optical coherence tomography. *Journal of Biomedical Optics*, 5(1), pp. 83-92.

Lai, J. et al., 2005. Experimental measurement of the refractive index of biological tissues by total internal reflection. *Applied Optics*, 44(10), pp. 1845-1849.

Li, H. and Xie, S., 1996. Measurement method of the refractive index of biotissue by total internal reflection. *Applied Optics*, 35(10), pp. 1793-1795.

Meglinski, I., 2015. *Biophotonics for Medical Applications.* s.l.:Elsevier.

Onofri, F. et al., 2007. Critical angle refractometry and sizing of bubble clouds. *Optics Letters*, 32(14), pp. 2070-2072.

Phibbs, M. K. and Giguère, P. A., 1951. Hydrogen Peroxide and its Analogues: I. Density, Refractive Index, Viscosity, and Surface Tension of Deuterium Peroxide - Deuterium Oxide Solutions. *Canadian Journal of Chemistry*, 29(2), pp. 173-181.

Sainov, S., 1994. Optical sensor based on total internal reflection diffraction grating. *Sensors and Actuators A: Physical*, 42(1), pp. 1-6.

Sani, E. and Dell'Oro, A., 2016. Spectral optical constants of ethanol and isopropanol from ultraviolet to far infrared. *Optical Materials*, Volumen 60, pp. 137-141.

SCHOTT North America, Inc, 2015. *Optical Glass Data Sheets.* s.l.:s.n.

Sliney, D. and Wolbarsht, M., 1980. *Safety with Lasers and Other Optical Sources: A comprehensive Handbook.* 1 ed. s.l.:Springer Science & Bussiness Media.

Uddin, S. Z. and Talukder, M. A., 2016. Reduction of Detection Volume in Total Internal Reflection Fluorescence Microscopy Using Graphene. *2016 9th International Conference on Electrical and Computer Engineering (ICECE).*

Wang, X. et al., 2016. *Progress in Planar Optical Waveguides.* Shangai: Springer.

Watad, I. et al., 2015. Critical-angle-based sensor with improved figure of merit using dip detection. *Optics Letters*, 40(19), pp. 4388-4391.

Yunus, W. M. M. et al., 2009. Refractive Index and Fourier Transform Infrared Spectra of Virgin Coconut Oil and Virgin Olive Oil. *American Journal of Applied Sciences*, 6(2), pp. 328-331.